All-conjugated donor-acceptor block copolymers featuring a pentafulvenyl-polyisocyanide-acceptor

Schraff, Sandra; Maity, Sudeshna; Schleeper, Laura; Dong, Yifan; Lucas, Sebastian; Bakulin, Artem A.; Von Hauff, Elizabeth; Pammer, Frank

published in
Polymer Chemistry
2020

DOI (link to publisher)
10.1039/c9py01879d

document version
Publisher's PDF, also known as Version of record

Volume 11
Number 11
21 March 2020
Pages 1823-1958

Polymer Chemistry

rsc.li/polymers

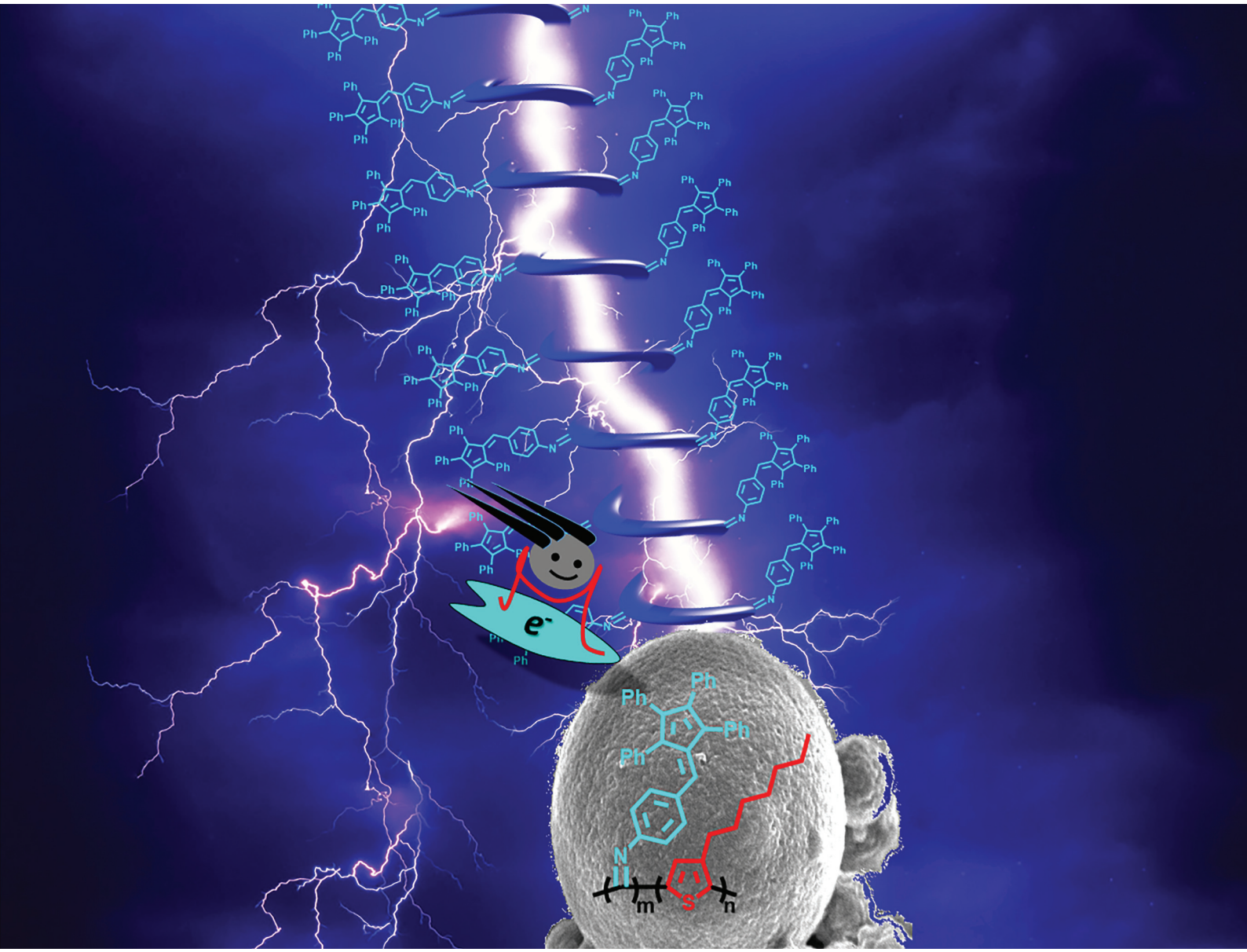

ISSN 1759-9962

ROYAL SOCIETY OF CHEMISTRY

PAPER

Elizabeth von Hauff, Frank Pammer *et al.*
All-conjugated donor–acceptor block copolymers featuring a pentafulvenyl-polyisocyanide-acceptor

Polymer Chemistry

ROYAL SOCIETY OF CHEMISTRY

PAPER

View Article Online
View Journal | View Issue

Cite this: *Polym. Chem.*, 2020, **11**, 1852

All-conjugated donor–acceptor block copolymers featuring a pentafulvenyl-polyisocyanide-acceptor†

Sandra Schraff,[a] Sudeshna Maity,[b] Laura Schleeper,[b,c] Yifan Dong,[c] Sebastian Lucas,[a] Artem A. Bakulin,[c] Elizabeth von Hauff *[b] and Frank Pammer *[a]

Received 13th December 2019,
Accepted 11th February 2020

DOI: 10.1039/c9py01879d

rsc.li/polymers

We report a fulvenyl-functionalized polyisocyanide (**PIC2**) with a high electron mobility of $\mu_e = 10^{-2}$ cm^2 V^{-1} s^{-1}. **PIC2** has been incorporated into block-copolymers with either regioregular poly(3-dodecylthiophene) (**P3DT → P(3DT-*b*-IC2)**) or regioregular polythiazole (**PTzTHX → P(TzTHX-*b*-IC2)**). Block copolymer batches with different block-sizes have been isolated and their properties have been studied. Fluorescence quenching in the solid state and transient absorption spectroscopy indicate energy transfer from the donor- to the acceptor block upon photo-excitation. Fabrication of proof-of-principle organic photovoltaic cells with **P(3DT-*b*-IC2)** gave cells with an open circuit voltage (V_{OC}) of *ca.* 0.89 V. The aggregation behavior of **P(3DT-*b*-IC2)** from solution was also studied, which revealed self-assembly into discreet microspheres of 1–8 μm diameter, with a size distribution of 1.72 (±0.37) μm under optimized aggregation conditions.

Introduction

Key challenges in the fabrication of organic solar cells (OSCs) are the control over the phase separation of the electron donor- (p-type) and the electron acceptor-material (n-type) in the active layer, as well as the long-term stability of the active layer morphology.[1] The self-organization of block copolymers (BCPs) has been proposed as an elegant way to reproducibly generate a stable bulk morphology,[2] due to the inherent ability of BCPs to phase separate into distinct phases on a nanometer scale. The potentialities of this approach were demonstrated, for instance by Thelakkat,[3] well as, by Russel and Emrick,[4] who showed that the phase separation of a poly(3-hexylthiophene)-*block*-poly(perylene diimide acrylate) can indeed be efficiently controlled. The key to the preparation of this block copolymer was the synthesis of the poly(3-hexylthiophene)-block (**P3HT**) *via* quasi-living cross-coupling polycondensation, different methods of which – termed Catalyst-Transfer-Polycondensation, CTP – have attracted increasing interest in recent years.[5] CTP has been used to generate chain-end functionalized conjugated polymers that can be converted into BCPs.[2a–d,g,3,4] Likewise, all-conjugated BCPs can be prepared *via* sequential addition of bifunctional monomers under CTP-conditions.[5] This approach has been extensive employed to prepare BCPs featuring different electron-rich building blocks, while few examples of all-conjugated donor–acceptor BCPs have been reported so far: Seferos and coworkers were able to add a poly(2*H*-benzotriazole) co-block to **P3HT** (**A**, Chart 1),[6] while Koeckelberghs *et al.* reported the preparation of BCP **B**, featuring a poly(thieno[3,4-*b*]pyrazine) co-block.[7,8]

Notably, when polythiophenes (**PT**s) are prepared by Kumada-coupling CTP, the reactive nickel-catalyst, that remains coordinated to the polymer chain-end, is also capable of polymerizing isocyanides and thereby allows to add a poly-

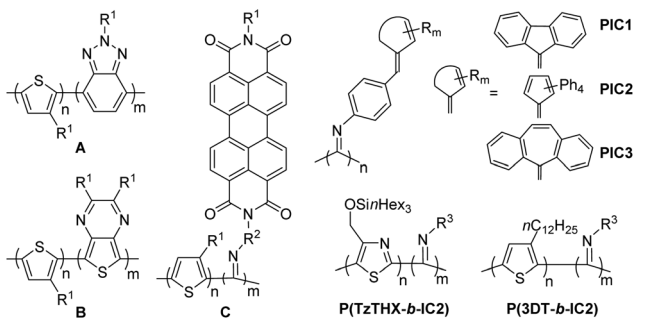

Chart 1 Examples for donor–acceptor BCPs (**A–C**), structure of homo polymers (**PIC1–3**) and BCPs reported herein. R^1 = alkyl, branched alkyl, $R^2 = -(CH_2)_6-$, $R^3 = -(C_6H_4)-CH{=}C_5Ph_4$.

[a]*Institute of Organic Chemistry II and Advanced Materials, University of Ulm, Albert-Einstein-Allee 11, 89081 Ulm, Germany. E-mail: frank.pammer@uni-ulm.de*
[b]*Department of Physics and Astronomy, Vrije Universiteit Amsterdam, De Boelelaan 1081, NL-1081 HV Amsterdam, Netherlands. E-mail: e.l.von.hauff@vu.nl*
[c]*Department of Chemistry, Imperial College London, London SW7 2AZ, UK*
†Electronic supplementary information (ESI) available. See DOI: 10.1039/c9py01879d

isocyanide (**PIC**[9]) co-block.[10] This discovery has led to an increased interest in polyarene and **PIC**-containing BCPs,[11,12] including the donor–acceptor BCP **C** (Chart 1), equipped with perylene diimide acceptor-groups.[13]

Until recently, OSCs based donor–acceptor-BCPs showed comparatively poor performance.[2a] However, significant progress in the last two years yielded power conversion efficiencies (PCE) exceeding 6%,[14] albeit with an active material that had been synthesized by coupling separately prepared alternating copolymers. In contrast, strategies for the preparation of new and structurally diverse BCPs by elegant sequential copolymerization remains challenging. In this work, we report significant progress towards this end, by introducing the first examples of all-conjugated donor–acceptor BCPs featuring a new type of **PIC** co-block as acceptor component.

In the recent past, we showed that regioregular polythiazoles (***rr*-PTz**s) can be prepared by CTP,[15–17] and developed a new class of electroactive **PIC**s equipped with conjugated fulvenyl-groups (Chart 1, **PIC1–PIC3**).[18] In this paper we report the charge transport characteristics of **PIC1**, **PIC2**, and **PIC3**, and the synthesis, and properties of donor–acceptor BCPs (**P(3DT-*b*-IC2)** and **P(TzTHX-*b*-IC2)**) featuring **PIC2** as acceptor-co-block.

Results and discussion

Semiconducting properties of fulvenyl-functionalized PICs

We investigated the charge transport abilities of the previously reported polymers **PIC1**, **PIC2** and **PIC3**,[18] in order to evaluate their potential use in organic electronic applications (see section 5.2 of the ESI†). To this end, a series of single carrier electron-only and hole-only devices was prepared, and the charge carrier mobilities were extracted by analyzing the current–voltage characteristics according to Space Charge Limited Current (SCLC) theory. These measurements yielded electron- (μ_e) and hole-mobilities (μ_h) in the suitable range for device fabrication of 10^{-4} to 10^{-5} cm^2 V^{-1} s^{-1} for all compounds. **PIC2** proved a surprising exception, however, as it showed a high electron transporting capability of μ_e = (1.04 ± 2.5) × 10^{-2} cm^2 V^{-1} s^{-1}. Indeed, to the best of our knowledge, this value is the highest electron mobility yet observed under SCLC conditions. Under comparable experimental conditions, electron mobilities above 10^{-3} cm^2 V^{-1} s^{-1} have been reported for high performance n-type acceptor polymers.[1,19] However, higher SCLC mobilities in the range of 10^{-2} to 10^{-1} cm^2 V^{-1} s^{-1} have only been reported for hole conducting (p-type) semiconducting polymers.[20] The origin of the high electron mobility in **PIC2** could not be ascertained at this point. **PIC2** does not melt prior to decomposition, and is amorphous, according to X-ray analyses.‡ Also, since all three **PIC**s are exclusively composed of conjugated π-systems, this lack of insulating alkyl-sidechains should be beneficial for charge transport in all cases. What makes **PIC2** unique, however, is the three-dimensional structure of the tetraphenylcyclopentadienyl-moiety.[18,21] Combined with the non-planar structure of the polyisocyanide backbone,[9] this may allow interdigitation of phenyl-rings of neighbouring polymer chains in three dimensions, and may thereby improve electronic coupling and charge hopping between chains.

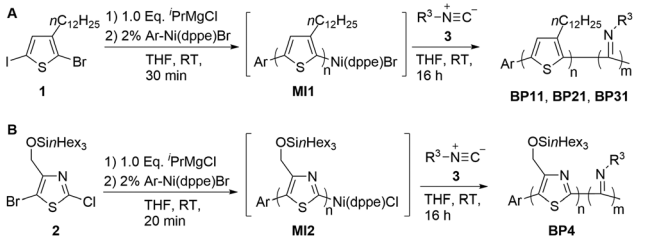

Scheme 1 Block-copolymer syntheses. Ar = 2-MeO-phenyl. For structure of R^3 see **PIC2** in Chart 1. **1** : **3** Feed ratios for **BP11**/**BP21**/**BP31** = 1 : 1, 2 : 1, and 3 : 1.

PIC2 undergoes reversible electrochemical reduction with a low LUMO-level of −3.60 eV,[18] and has a large optical gap (λ_{onset} = 560 nm, E_g^{opt} = 2.27 nm), which indicates a HOMO-level of *ca.* −5.85 eV. This combination should make **PIC2** suitable for use as n-type acceptor co-block in combination with **PT**s and other electron rich donors. We therefore further explored the potentialities of **PIC2** by preparing the corresponding BCPs with poly(3-dodecylthiophene) (**P3DT** → **P(3DT-*b*-IC2)** and poly(4-((trihexylsilyloxy)-methylene)-thiazole) (**PTzTHX**[17] → **P(TzTHX-*b*-IC2)**.

PIC2-containing block-copolymers

In a one-pot reaction, macroinitiators (**MI1**, **MI2**) bearing *ortho*-anisyl- and Ni(II)-end-groups were prepared from 2-bromo-3-dodecyl-5-iodo-thiophene (**1**)[22] and 5-bromo-2-chloro-4-((trihexylsilyloxy)-methylene)-thiazole (**2**),[15] *via* Kumada-coupling CTP using 2% Ni(*o*-anisyl)(dppe)Br[15] as pre-catalyst (Scheme 1, dppe = 1,2-bis(diphenylphosphino)ethane). The polymerization was left to proceed for 20–30 minutes, and the isocyanide **3** was then added in different ratios (Table 1) to generate the **PIC** co-block. Subsequently, the BCPs were isolated by precipitation into methanol, and were purified by washing and extraction with different solvents.§

Analyses of the BCP batches by gel permeation chromatography (GPC) gave number-average molecular weights of M_n = 22.9 kg mol^{-1} at a polydispersity (PDI) of 1.06 for **BP11**, and M_n = 24.5 kg mol^{-1} (PDI = 1.03) and 21.4 kg mol^{-1} (PDI = 1.03) for **BP21** and **BP31**, respectively (see Fig. S1a/b in the ESI†). Control-samples of the macroinitiators **MI1** taken prior to addition of the isocyanide showed M_n values of 15.7 kg mol^{-1}

‡ So far, powder X-ray diffraction on bulk samples and grazing incidence X-ray diffraction on films did not yield refraction signals that would indicate crystallinity or larger scale ordering.

§ **BP11**/**BP21**/**BP31**: Washed with methanol, acetone and hexane, followed by extraction with dichloromethane (**BP11**) or chloroform (**BP21**/**BP31**). **BP4**: Washed with methanol and acetone. Crude **BP4** extracted with hexane followed by purification *via* preparative GPC.

Table 1 Physical properties of BCPs. For more complete data and experimental details see Tables S1 and S2 in the ESI†

BCP	Feed ratio 1,2/3	MI1/MI2 Mn^{GPC} [kg mol^{-1}]	PDI	BCP Mn^{GPC} [kg mol^{-1}]	PDI	$n:m$ GPC	$n:m$ NMR	$n:m$ EDX	% PIC[b]	λ_{max}^{sol} [c] [nm]	λ_{onset}^{sol} [c] [nm]	λ_{max}^{film} [c] [nm]	λ_{onset}^{film} [c] [nm]
BP11	1/1	15.7	1.05	22.9	1.06	63 : 15	50 : 59	1 : 2	70	380	550	605	649
BP21	2/1	20.8	1.02	24.5	1.03	83 : 8	53 : 42	2 : 1	60	406	533	605	650
BP31	3/1	20.8	1.02	21.4	1.03	83 : 1	53 : 8	4.5 : 1	23	441	539	610[d]	653
BP4[a]	1/1	33.6	1.13	38.4	1.04	85 : 10	89 : 39	5.7 : 1	35	483	545	545	578

[a] After purification by preparative GPC. [b] Mass% of **PIC2** in the BCP based on ^{1}H NMR data. [c] UV-vis-absorption data in DCM-solution: λ_{max}(**PIC2**) = 368 nm, λ_{onset}(**PIC2**) = 560 nm;[18] λ_{max}(**P3DT**) = 445 nm; λ_{onset}(**P3DT**) = 545 nm; λ_{max}(**PTzTHX**) = 486 nm, λ_{onset}(**PTzTHX**) = 545 nm.[17b] [d] Longest-wavelength absorption band determined by Gaussian deconvolution.

(PDI = 1.05) for **BP11**, and 20.8 kg mol^{-1} (PDI = 1.02) for **BP21** and **BP31**, which were prepared in a combined experiment.¶ For **BP4** a similar increase of the molecular weight was achieved from M_n = 33.6 kg mol^{-1} (PDI = 1.13) for the macroinitiator **MI2** to M_n = 38.4 kg mol^{-1} (PDI = 1.04) in **BP4**. The reaction was not quite as clean, however, and the crude polymer required additional purification by preparative GPC (Fig. S2 in the ESI†). The GPC data show a direct correlation of the BCP-composition to the feed ratio in **BP11** through **BP31** (Table 1), in so far as the lengths of the **PIC**-blocks decreases with the lowered thiophene (n) to isocyanide (m) ratio. However, GPC seemingly underestimates the incorporation of isocyanide **3**. For instance, a thiophene : isocyanide feed ratio of 1 : 1 results in an $n:m$ ration of 4 : 1 ratio in **BP11**, while for **BP31** the GPC data correspond to addition of only one isocyanide monomer per polymer chain. We attribute this finding to the known overestimation of the MW of the rod-like **PT**s by GPC.[23] In the present case, this is then compensated by addition of the bulkier isocyanides in the **PIC2**-co-block.‖ This conjecture was corroborated by energy dispersive X-ray-spectroscopy (EDX), and end-group analyses *via* ^{1}H NMR, as well as thermal analyses: an estimate of the degree of polymerization by referencing the aryl- and alkyl-signals in ^{1}H NMR spectra against the *o*-anisyl-groups introduced at the polymer chain end,[15]** (Table 1, see Fig. S3 through S5 in the ESI†) gave invariably lower MWs for the **P3DT**- and **PTzTHX**-blocks, and showed 4–8-times larger **PIC**-contents. Likewise, determination of the sulphur- and nitrogen-content of aggregated BCPs by EDX-analyses (Table 1, see also Table S2 in the ESI†) gave molar n/m ratios that are in good agreement with the values derived from ^{1}H NMR data.

Thermal analyses: analysis by thermal gravimetry (TGA, Fig. S6 and Table S1 in the ESI†) shows that **PIC2** degrades above 365 °C and leaves 43% residual mass at 800 °C. The homo polymers **P3DT** and **PTzTHX** decompose rapidly above 457 °C and 408 °C to leave just 17% and 14% of residual mass, respectively. Sequential decomposition of the individual blocks of the BPCs could not be directly observed. However, the residual masses of the BCPs at 800 °C directly correlate with the relative content of **PIC2**, for both types of BCPs. The homo- and block-copolymers were also analysed by differential scanning calorimetry (DSC, Fig. S7†). **PIC2** decomposes without melting,[18] while for **P3DT** melting (T_m = 165 °C) and crystallization (T_c = 135 °C) was observed in agreement with literature.[24] Phase transitions of the **P3DT**-block were observed at increasingly lower temperatures for **BP31** (T_m = 165 °C, T_c = 108 °C) and **BP21** (T_m = 147 °C, T_c = 97 °C), while for **BP11** no phase transitions were observed. The phase-transitions in the block-copolymer were unambiguously assigned to crystallization of the **P3DT**-block by subsequent analyses of the DSC samples of **BP31** and of a **P3DT**-reference sample by small- and wide-angle powder X-ray diffraction (PXRD). Both samples show a diffraction peaks at 2Θ = 3.56° that correspond to a distance of 24.7 Å, as expected for the lamellar spacing of the PT main chains in **P3DT**[26] (see Fig. S15 in the ESI†). Weaker refraction peaks assigned to π–π-stacking are also present at 23.0° (3.95 Å).

Notably, according to these data, all BCPs have an appreciable **PIC2**-content, ranging from 23 mass% for **BP31** to 70 mass% for **BP11**, all of which is π-conjugated material that can contribute to charge transport.

UV-vis absorption spectra of the BCP also allow to deduce their composition. **PIC2** has a longest wavelength absorption maximum (λ_{max}) in solution at 365 nm, while the λ_{max} of **P3DT** is 445 nm. Consequently, the absorption maxima of **BP11** through **BP31** the increasingly shift to longer wave-length (Fig. 1A) with increasing content of **P3DT**. This assumption about the origin of the red-shift was corroborated by reproduction of the BCP absorption spectra through overlay of spectra

¶A macroinitiator was prepared by polymerization from dihalothiophene **1**. The resulting solution was divided into two parts, which were treated with different relative amounts of isocyanide **3**.

‖The rod-like character of **PT**s inflates their effective hydrodynamic volume, and thus leads to an overestimation of their molecular weight by GPC. In contrast **PIC**s adopt a non-planar conformation that significantly reduces the linear chain-extension per repeat unit. In a tightly packed 4_1 helix (one full turn per four repeat units) addition of 4 monomers would extend the polymer chain by *ca.* 3 Å, compared to *ca.* 3.4 Å per thienyl-ring in **PT**s. Additionally, monomer **3** also adds considerable bulk to the periphery of the polymer. GPC results for the hexane-soluble **PTzTHX** are much more representative due to the bulk of its side-chains. For GPC-analyses of **PTz**s see also ref. 15.

**We have previously reported the molecular weight determination of anisyl-capped PTzs *via* ^{1}H NMR. See ref. 15 for details. The same method can be employed to determine the molecular weight of anisyl-capped P3DT. For reference, spectra of anisyl-capped P3DT homopolymers have been included in Fig. S5 of the ESI.†

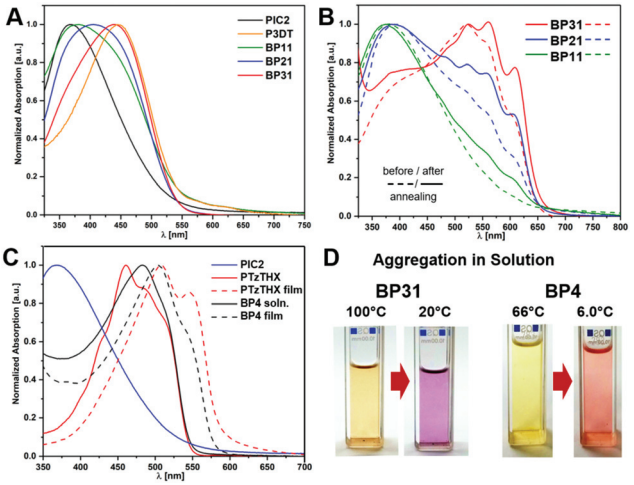

Fig. 1 A–C: UV-vis absorption of **BP11**, **BP21**, and **BP31** and **BP4** in DCM solution, and of annealed films. Spectra of **P3DT**, **PTzTHX**, and **PIC2** included for reference. D: Color change of BCPs upon aggregation in solution.

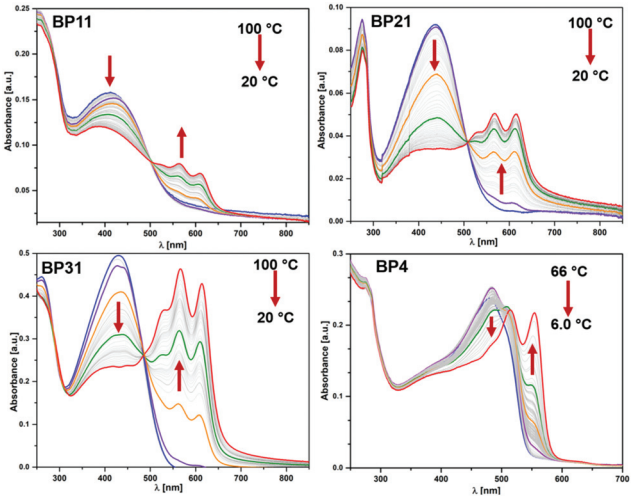

Fig. 2 Aggregation of **BP11**, **BP21**, and **BP31** in *n*-heptane solution monitored by UV-vis absorption spectroscopy.

of the respective homopolymers (see Fig. S13 in the ESI†). Film spectra also allowed to directly observe the **P3DT**-block (Fig. 1B). As-cast films of the BCPs show new red-shifted absorption bands compared to solution, that exhibit with weak vibronic structuring. The relative intensity of the newly emerging band scales with **P3DT**-content, and the vibronic structuring becomes more pronounced after annealing, indicating crystallization of the **P3DT** block.[26] However, an investigation of the annealed films by Gracing Incidence X-ray Diffraction (GIXD), showed no refraction that would indicate the presence of separate crystalline phases. For **BP4** the presence of the **PIC2** block has a only a limited impact on the absorption spectra. Its main contribution is increased absorption of **BP4** below 450 nm.

The BCPs remained fluorescent in solution and showed emission corresponding to the respective **P3DT**- and **PTzTHX**-blocks, while in all cases fluorescence was quantitatively quenched in thin films (see Fig. S8A/B in the ESI†). Since **PIC2** is inherently non-fluorescent,[18] and both **PT**s[25] and **PTzTHX**[17] exhibit fluorescence in the solid state. This indicates that intramolecular charge-transfer onto the acceptor block does not occur in solution, but may be present in films.

The bulk morphology of the active layer is one of the most important factors determining the performance of organic photovoltaic cells. However, since GIXD investigations of films did not indicate the occurrence of phase-separation, we investigated the potential self-assembly of the BCPs in solution. **PIC2** is insoluble in *n*-alkanes, while **PTzTHX** and **P3DT** can be dissolved in these solvent at ambient to elevated temperatures. **BP11** through **BP4** were therefore each dissolved in hot *n*-heptane or *n*-hexane, and changes to the optical properties during slow cooling where continuously monitored by absorption and fluorescence spectroscopy (Fig. 1D, Fig. 2, see Fig. S9–S12 in the ESI†). All BCPs initially appear molecularly dissolved, but begin to aggregate below 55–60 °C. For **BP11** through **BP31**, the characteristic absorption bands of the **PT**-block emerge, accompanied by a weakening of the corresponding band of the molecularly dissolved polymer fraction between 300 and 500 nm. This process reveals isosbestic points (IPs) for all three **PT**-containing BCPs between 486 and 509 nm (**BP11**: λ_{IP} = 505 nm, **BP21**: λ_{IP} = 509 nm, and **BP31**: λ_{IP} = 486 nm). In the aggregation of neat **P3DT** an IP is also observed at 486 nm (Fig. S9 in the ESI†). The effect is attributed to serendipitous compensation of the higher absorption coefficient of the aggregated polymer against the lowering concentration of the solubilized polymer. The underlying absorption of the **PIC2**-block hardly changes between solution and solid state,[18] but causes the shift of the IP longer wavelength with increasing **PIC2**-content. Furthermore, the relative intensity of the aggregation bands again directly scales with the relative **P3DT**-content, while the vibronic fine-structures are much more sharper than those observed in film spectra (Fig. 1B). This latter observation indicated the presence of structurally well-defined aggregates, and prompted us to analyze the aggregated BCPs in more detail. PXRD of aggregated precipitates revealed low overall crystallinity (see Fig. S13A/B in the ESI†). However, refraction peaks associated with the lamellar spacing of **P3DT**[26] at $2\Theta \approx 3.75°$ (23.6 Å) indicate the presence of crystalline **P3DT** in aggregated **BP11** and **BP21**.

Further analyses of the aggregates by Scanning Electron Microscopy (SEM) showed **BP11** and **BP21** to form unspecific aggregates, without larger scale ordering (see section 4 of the ESI†). **BP31**, on the other hand, reproducibly self-assembled into microspheres with sizes ranging from 0.5 to 5 μm (Fig. 3E–G, and section 4 of the ESI†). An analysis of the size distribution showed the BCP-particles to have an average diameter of 5.33 μm with a broad standard deviation of σ = ±1.28 μm (Fig. 3H), along with a significant portion of unspecifically aggregated material similar to **BP21**. Slower cooling of a more dilute solution allowed better control over the particle formation, and resulted in microspheres with an average dia-

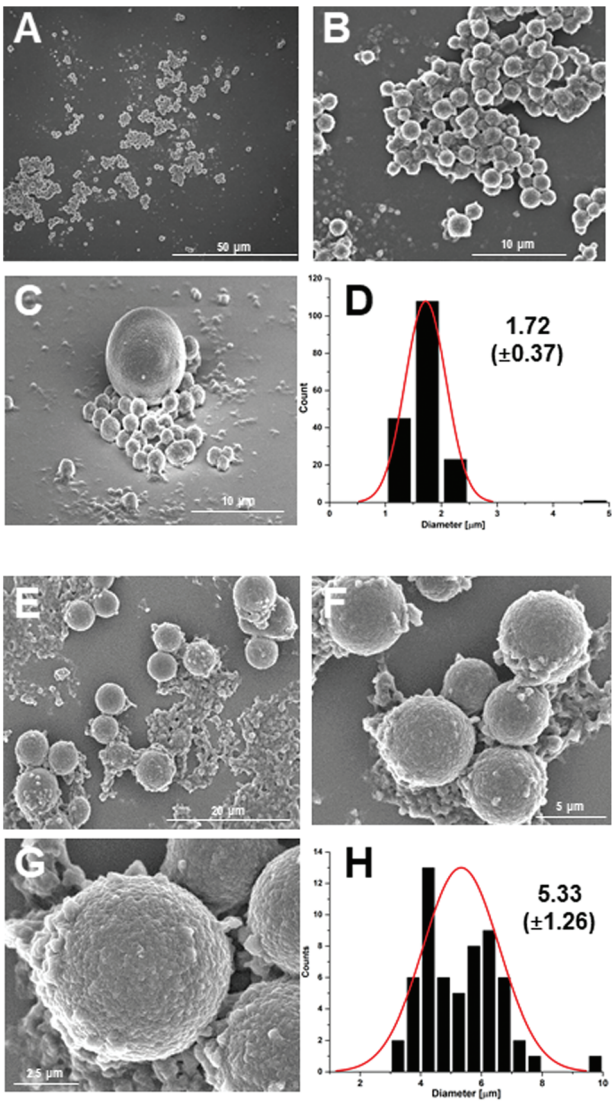

Fig. 3 SEM-micrographs (A–C, E–G) and size histograms (D/H) of microspheres formed by self-assembling of **BP31** under different conditions.

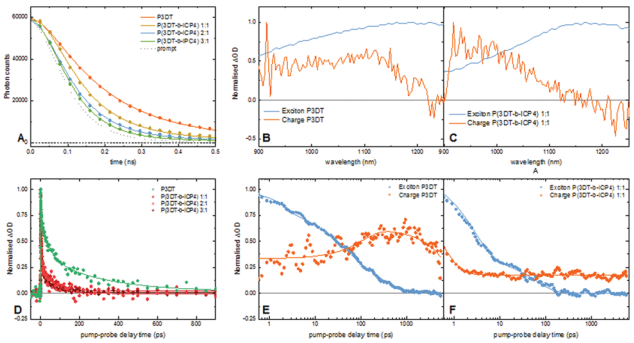

Fig. 4 Transient absorption spectroscopy data for **BP11**, **BP21** and **BP31**. A: Time-resolved photo luminescence decay. B/C: Exciton-and charge-generation in **P3DT** and **BP11**. D: Kinetics of photo luminescence decay. E/F: Kinetics of exciton- and charge-generation derived by global analysis of transient absorption spectra with charge as reference.

meter of 1.72 μm (σ = ±0.37 μm) and a much narrower size distribution (Fig. 3A–D).

Analogous aggregation experiments with **BP4** also confirmed aggregation of the **PTzTHX**-block (Fig. 2, see also Fig. S10 through S12 in the ESI† [17]). Initially, absorption and fluorescence correspond to those of neat **PTzTHX** in solution, while lowering of the temperature yields spectra that correspond to **PTzTHX** in the solid state. Hence, these observations indicate that charge transfer from **PTzTHX** to the **PIC2**-block is not taking place in the polymer aggregates. Analyses of these aggregates by SEM did not show distinct aggregate formation.

Time-resolved fluorescence, transient absorption spectroscopy, and block-copolymer solar cells

Time resolved fluorescence measurements by time-correlated single photon counting (TCSPC, see ESI† for details) on **BCP** films, showed faster fluorescence quenching in **BP11**, **BP21** and **BP31** than in neat **P3DT**. We interpret this as a clear evidence of electron transfer from **P3DT** to the **PIC2**-acceptor block (Fig. 4A). Curiously, fluorescence quenching was faster in **BP21** and **BP31**, in spite of the lower acceptor content in these polymers. A reason for this observation may be a higher crystallinity of the **P3DT**-phase in these materials, which would also lead to more self-quenching than in **BP11**.

The fluorescence quenching results are confirmed by transient absorption experiments (Fig. 4D). Global analysis of transient absorption data for neat **P3DT** (Fig. 4B/E) showed the decay of excitons on a ~50 ps timescale with a very small number of excitons being converted to geminate charge pairs, which also decays on the ~ns timescale. **BP11** (Fig. 4C/F) in contrast shows faster decay for excitons assisted with appearance of a polaron signal. This indicates efficient exciton dissociation to charges at ~2 ps timescale. Photo-generated carriers in **BP11** are much less prone to recombination in agreement with the observed photocurrent generation in photovoltaic devices. Overall, ultrafast experiments indicate very efficient early stages of photon-to-charge conversion in all the studied block-copolymer materials.

Tests of all three BCPs in single-component photovoltaic cells gave the best performance (see section 5.1 of the ESI† for details) for a device fabricated from **BP21**. **BP21** showed a maximum power conversion efficiency (PCE) of 0.01% at an open circuit voltage (V_{OC}) of 0.65 V, a short circuit current (I_{SC}) of 66.2 μA cm^{-2} and a fill factor (FF) of 30%. **BP11** gave the highest V_{OC} (0.89 V), but showed much lower overall performance (PCE = 0.005%) due to a lower I_{SC} (24.4 μA cm^{-2}) and a moderate FF (25%). **BP31** showed an intermediate performance (PCE = 0.008%), due to a lower V_{OC} (0.48 V), and a reasonably I_{SC} (56.9 μA cm^{-2}). Device performance generally improved upon thermal or solvent vapour annealing (see ESI† for details), which indicates that all devices benefit from crystallization of the **P3DT**-phase. The results highlight the importance of the relative donor- and acceptor content in the BCO, which appears to be best in **BP21**. Too low **P3DT** content in

BP11 may hamper hole extraction and also phase separation, since **PIC2** does not melt. While the lower content of **PIC2** in **BP31** does not provide percolation pathways for electron transport. The reason for the low performance seems to be inefficient donor–acceptor phase-separation in the active layer, which prevents charge extraction and favours recombination.

These results show that the combination of **PIC2** with a **PT** is a viably strategy to generate functioning OSCs. However, given the known challenges in development of BCP-based organic solar cells, further optimization will be required to improve the performance of systems reported herein.

Conclusions

We have established fulvenyl-functionalized **PIC**s, as a promising new class of semiconducting polymers. Particularly the electron mobility exhibited by the acceptor-polymer **PIC2** (μ_e = 1.04×10^{-2} (±2.5) $cm^2\ V^{-1}\ s^{-1}$) rivals that of known high performance polymeric n-type semiconductors. Furthermore, we have shown, that **PIC2** can be readily incorporated into all-conjugated BCPs (**P(3DT-*b*-IC2)** and **P(TzTHX-*b*-IC2)**) with **PT**- and **PTz** co-blocks that are accessible *via* nickel catalyzed cross-coupling polycondensation. Fluorescence quenching in BCP-films, and transient absorption spectroscopy data indicate energy transfer from the donor- onto the acceptor-blocks upon photoexcitation. Preparation of proof-of-principle-devices also indicates that **P(3DT-*b*-IC2)** is a promising material for the fabrication of single-component block-copolymer solar cells. Investigation of the aggregation behaviour of **P(3DT-*b*-IC2)** showed that its self-organization can be controlled by varying the relative block-sizes, and aggregation conditions. These findings show that fulvenyl-functionalized **PIC**s constitute a highly versatile class of new electroactive polymers that may be employed in various organic electronic applications.

Conflicts of interest

There are no conflicts to declare.

Acknowledgements

AAB is a Royal Society University Research Fellow. We thank Prof. Paul Walther, Reinhard Weih, and Gregor Neusser at U. Ulm for assistance with SEM-, TEM- and EDX-measurements.

Notes and references

1 (*a*) H. Kang, W. Lee, J. Oh, T. Kim, C. Lee and B. J. Kim, From Fullerene – Polymer to All-Polymer Solar Cells: The Importance of Molecular Packing, Orientation, and Morphology Control, *Acc. Chem. Res.*, 2016, **49**, 2424; (*b*) C. R. McNeill, Morphology of all-polymer solar cells, *Energy Environ. Sci.*, 2012, **5**, 5653.

2 (*a*) J. Roncali and I. Grosu, The Dawn of Single Material Organic Solar Cells, *Adv. Sci.*, 2019, **6**, 1801026; (*b*) D. J. Jones and V. D. Mitchell, Advances toward the effective use of block copolymers as organic photovoltaic active layers, *Polym. Chem.*, 2018, **9**, 795; (*c*) J. Wang and T. Higashihara, Synthesis of all-conjugated donor–acceptor block copolymers and their application in all-polymer solar cells, *Polym. Chem.*, 2013, **4**, 5518; (*d*) Z. Lin, Conjugated rod–coil and rod–rod block copolymers for photovoltaic applications, *J. Mater. Chem.*, 2011, **21**, 17039; (*e*) M. Sommer, S. Huettner and M. Thelakkat, Donor–acceptor block copolymers for photovoltaic application, *J. Mater. Chem.*, 2010, **20**, 10788; (*f*) R. A. Segalman, B. Mcculloch, S. Kirmayer and J. J. Urban, Block Copolymers for Organic Optoelectronics, *Macromolecules*, 2009, **42**, 9205; (*g*) U. Scherf, S. Adamczyk, A. Gutacker and N. Koenen, All-Conjugated, Rod-Rod Block Copolymers-Generation and Self-Assembly Properties, *Macromol. Rapid Commun.*, 2009, **30**, 1059.

3 (*a*) M. Sommer, A. S. Lang and M. Thelakkat, Crystalline-crystalline donor-acceptor block copolymers, *Angew. Chem., Int. Ed.*, 2008, **47**, 7901; (*b*) S. Huettner, J. M. Hodgkiss, M. Sommer, R. H. Friend, U. Steiner and M. Thelakkat, Morphology-Dependent Charge Photogeneration in Donor–Acceptor Block Copolymer Films Based on Poly (3-hexylthiophene)-*block* -Poly(perylene bisimide acrylate), *J. Phys. Chem. B*, 2012, **116**, 10070; (*c*) R. H. Lohwasser, G. Gupta, P. Kohn, M. Sommer, A. S. Lang, T. Thurn-Albrecht and M. Thelakkat, Phase Separation in the Melt and Confined Crystallization as the Key to Well-Ordered Microphase Separated Donor–Acceptor Block Copolymers, *Macromolecules*, 2013, **46**, 4403; (*d*) C. D. Heinrich, M. Fischer, T. Thurn-Albrecht and M. Thelakkat, Modular Synthesis and Structure Analysis of P3HT-*b*-PPBI Donor–Acceptor Diblock Copolymers, *Macromolecules*, 2018, **51**, 7044.

4 Q. Zhang, A. Cirpan, T. P. Russell and T. Emrick, Donor–Acceptor Poly(thiophene-*block*-perylene diimide) Copolymers: Synthesis and Solar Cell Fabrication, *Macromolecules*, 2009, **42**, 1079.

5 (*a*) *Semiconducting Polymers: Controlled Synthesis and Microstructure*, ed. D. Seferos, L. Pozzo and M. Ueda, RSC Polymer Chemistry, Cambridge, 2016, ISBN-13: 978-1782620341; (*b*) M. A. Baker, C.-H. Tsai and K. J. T. Noonan, Strategies, Catalysts and Monomers for the Controlled Synthesis of Conjugated Polymers, *Chem. – Eur. J.*, 2018, **24**, 13078; (*c*) A. K. Leone and A. J. McNeil, Matchmaking in Catalyst-Transfer Polycondensation: Optimizing Catalysts based on Mechanistic Insight, *Acc. Chem. Res.*, 2016, **49**, 2822; (*d*) T. Yokozawa and Y. Ohta, Transformation of Step-Growth Polymerization into Living Chain-Growth Polymerization, *Chem. Rev.*, 2015, **116**, 1950; (*e*) Z. J. Bryan and A. J. McNeil, Conjugated Polymer Synthesis via Catalyst-Transfer Polycondensation (CTP):

Mechanism, Scope, and Applications, *Macromolecules*, 2013, **46**, 8395; (*f*) T. Yokozawa and A. Yokoyama, Chain-Growth Condensation Polymerization for the Synthesis of Well-Defined Condensation Polymers and π-Conjugated Polymer, *Chem. Rev.*, 2009, **109**, 5595.

6 C. R. Bridges, H. Yan, A. A. Pollit and D. S. Seferos, Controlled Synthesis of Fully π-Conjugated Donor–Acceptor Block Copolymers Using a Ni(II) Diimine Catalyst, *ACS Macro Lett.*, 2014, **3**, 671.

7 P. Willot, D. Moerman, P. Leclère, R. Lazzaroni, Y. Baeten, M. Van der Auweraer and G. Koeckelberghs, One-Pot Synthesis and Characterization of All-Conjugated Poly (3-alkylthiophene)-*block*-poly(dialkylthieno[3,4-*b*]pyrazine), *Macromolecules*, 2014, **47**, 6671.

8 Poly(thieno[3,4-*b*]pyrazine) is a low band gap polymer ($E_g^{opt} \approx 1.0$ eV) with high electron affinity (LUMO ≈ −4.1 eV), but also a very high HOMO-level (*ca.* −5.1 eV), which renders it unsuitable *e.g.* as acceptor material in OPV.

9 (*a*) E. Schwartz, M. Koepf, H. J. Kitto, R. J. M. Nolte and A. E. Rowan, Helical Polyisocyanides: Past, Present and Future, *Polym. Chem.*, 2011, **2**, 33; (*b*) Y. Nagata and M. Suginome, *Polyisocyanides, Poly(quinoxaline-2,3-diyl)s, and Related Helical Polymers Used as Chiral Polymer Catalysts in Asymmetric Synthesis in Polymeric Chiral Catalyst Design and Chiral Polymer Synthesis*, ed. S. Itsuno, John Wiley and Sons, Hoboken, 2011, p. 223; (*c*) R. J. M. Nolte, Helical Polyisocyanides, *Chem. Soc. Rev.*, 1994, **23**, 11; (*d*) F. Millich, Polymerization of Isocyanides, *Chem. Rev.*, 1972, **72**, 101.

10 (*a*) T. Yamada and M. Suginome, Synthesis of Helical Rod-Coil Multiblock Copolymers by Living Block Copolymerization of Isocyanide and 1,2-Diisocyanobenzene Using Arylnickel Initiators, *Macromolecules*, 2010, **43**, 3999; (*b*) Z.-Q. Wu, R. J. Ono, Z. Chen and C. W. Bielwaski, Synthesis of Poly(3-alkylthiophene)-*block*-poly(arylisocyanide): Two Sequential, Mechanistically Distinct Polymerizations Using a Single Catalyst, *J. Am. Chem. Soc.*, 2010, **132**, 14000.

11 (*a*) Z.-Q. Wu, D.-F. F. Liu, Y. Wang, N. Liu, J. Yin, Y.-Y. Y. Zhu, L.-Z. Z. Qiu and Y.-S. S. Ding, One Pot Synthesis of a Poly(3-hexylthiophene)-*b*-poly(quinoxaline-2,3-diyl) Rod-Rod Diblock Copolymer and its Tunable Light Emission Properties, *Polym. Chem.*, 2013, **4**, 4588; (*b*) Z. Yu, N. Liu, L. Yang, Z. Jiang and Z. Wu, One-Pot Synthesis, Stimuli Responsiveness, and White-Light Emissions of Sequence-Defined ABC Triblock Copolymers Containing Polythiophene, Polyallene, and Poly(phenylisocyanide), *Macromolecules*, 2017, **50**, 3204; (*c*) M. Su, N. Liu, Q. Wang, H. Wang, J. Yin and Z.-Q. Wu, Facile Synthesis of Poly (phenyleneethynylene)-*block*-Polyisocyanide Copolymers via Two Mechanistically Distinct, Sequential Living Polymerizations Using a Single Catalyst, *Macromolecules*, 2016, **49**, 110; (*d*) Z.-Q. Wu, J. D. Radcliffe, R. J. Ono, Z. Chen, Z. Li and C. W. Bielawski, Synthesis of Conjugated Diblock Copolymers: Two Mechanistically Distinct, Sequential Living Polymerizations Using a Single Catalyst, *Polym. Chem.*, 2012, **3**, 874; (*e*) L. Xu, X.-H. Xu, N. Liu, H. Zou and Z.-Q. Wu, A Facile Synthetic Route to Multifunctional Poly(3-hexylthiophene)-*b*-poly(phenyl isocyanide) Copolymers: From Aggregation-Induced Emission to Controlled Helicity, *Macromolecules*, 2018, **51**, 7546.

12 O. Coulembier, M. Surin, A. Mehdi, R. Lazzaroni, R. C. Evans and P. Dubois, Expanding the light absorption of poly(3-hexyl-thiophene) by end-functionalization with π-extended porphyrins, *Chem. Commun.*, 2016, **52**, 171.

13 R. J. Ono, A. D. Todd, Z. Hu, D. A. Vanden Bout and C. W. Bielawski, Synthesis of a Donor-Acceptor Diblock Copolymer via Two Mechanistically Distinct, Sequential Polymerizations Using a Single Catalyst, *Macromol. Rapid Commun.*, 2014, **35**, 204.

14 S. H. Park, Y. Kim, N. Y. Kwon, Y. W. Lee, H. Y. Woo, W.-S. Chae, S. Park, M. J. Cho and D. H. Choi, Significantly Improved Morphology and Efficiency of Nonhalogenated Solvent-Processed Solar Cells Derived from a Conjugated Donor–Acceptor Block Copolymer, *Adv. Sci.*, 2020, **7**, 1902470.

15 F. Pammer, J. Jäger, B. Rudolf and Y. Sun, Soluble Head-to-Tail Regioregular Polythiazoles: Preparation, Properties and Evidence for Chain-Growth Behavior in the Synthesis via Kumada-Coupling Polycondensation, *Macromolecules*, 2014, **47**, 5904.

16 M. L. Smith, A. K. Leone, P. M. Zimmerman and A. J. McNeil, Impact of Preferential π–Binding in Catalyst-Transfer Polycondensation of Thiazole Derivatives, *ACS Macro Lett.*, 2016, **5**, 1411.

17 J. Jäger, N. Tchamba Yimga, M. Urdanpilleta, E. von Hauff and F. Pammer, Towards n-Type Analogues to Poly (3-alkylthiophene)s: Influence of Side-chain Variation on Bulk-morphology and Electron Transport Characteristics of Head-to-tail Regioregular Poly(4-alkylthiazole)s, *J. Mater. Chem. C*, 2016, **4**, 2587.

18 S. Schraff, Y. Sun and F. Pammer, Fulvenyl-functionalized Polyisocyanides – Cross-conjugated Electrochromic Polymers With Variable Optical and Electrochemical Properties, *Macromolecules*, 2018, **51**, 5323.

19 R. Steyrleuthner, R. Di Pietro, B. A. Collins, F. Polzer, S. Himmelberger, M. Schubert, Z. Chen, S. Zhang, A. Salleo, H. Ade, A. Facchetti and D. Neher, The Role of Regioregularity, Crystallinity, and Chain Orientation on Electron Transport in a High-Mobility n-Type Copolymer, *J. Am. Chem. Soc.*, 2014, **136**, 4245.

20 M. Nikolka, K. Broch, J. Armitage, D. Hanifi, P. J. Nowack, D. Venkateshvaran, A. Sadhanala, J. Saska, M. Mascal, S.-H. Jung, J.-K. Lee, I. McCulloch, A. Salleo and H. Sirringhaus, High-mobility, trap-free charge transport in conjugated polymer diodes, *Nat. Commun.*, 2019, **10**, 2122.

21 S. Schraff, Y. Sun, A. Orthaber and F. Pammer, Gold(I) Complexes of Fulvenyl-functionalized Arylisocyanides", *Eur. J. Inorg. Chem.*, 2019, 42–50.

22 R. S. Loewe, P. C. Ewbank, J. Liu, L. Zhai and R. D. McCullough, Regioregular, Head-to-Tail Coupled Poly (3-alkylthiophenes) Made Easy by the GRIM Method:

Investigation of the Reaction and the Origin of Regioselectivity, *Macromolecules*, 2001, **34**, 4324.

23 M. Wong, J. Hollinger, L. M. Kozycz, T. M. McCormick, Y. Lu, D. C. Burns and D. S. Seferos, An apparent size-exclusion quantification limit reveals a molecular weight limit in the synthesis of externally initiated polythiophenes, *ACS Macro Lett.*, 2012, **1**, 1266.

24 V. Causin, C. Marega and A. Marigo, Crystallization and, Melting Behavior of Poly(3-butylthiophene), Poly(3-octylthiophene), and Poly(3-dodecylthiophene), *Macromolecules*, 2005, **38**, 409.

25 Z. Hu, A. P. Willard, R. J. Ono, C. W. Bielawski, P. J. Rossky and D. A. Vanden Bout, An insight into non-emissive excited states in conjugated polymers, *Nat. Commun.*, 2015, **6**, 8246.

26 P.-T. Wu, H. Xin, F. S. Kim, G. Ren and S. A. Jenekhe, Regioregular Poly(3-pentylthiophene): Synthesis, Self-Assembly of Nanowires, High-Mobility Field-Effect Transistors, and Efficient Photovoltaic Cells, *Macromolecules*, 2009, **42**, 8817.